

Sample Distortion for Compressed Imaging

Chunli Guo*, *Student Member, IEEE*, and Mike E. Davies, *Senior Member, IEEE*

Institute for Digital Communications

Joint Research Institute for Signal and Image Processing

School of Engineering

The University of Edinburgh

EH9 3JL, Edinburgh, UK

{c.guo, mike.davies}@ed.ac.uk

Abstract—We propose the notion of sample distortion function for i.i.d compressive distributions with the aim to fundamentally quantify the achievable reconstruction performance of compressed sensing for certain encoder-decoder pairs at a given undersampling ratio. The theoretical SD function is derived for the Gaussian encoder and Bayesian optimal approximate message passing decoder thanks to the rigorous analysis of the AMP algorithm. We also show the convexity of the general SD function and derive two lower bounds. We then apply the SD framework to analyse compressed sensing for natural images using a multi-resolution statistical image model with both generalized Gaussian distribution and the two-state Gaussian mixture distribution. For this scenario we are able to achieve an optimal bandwise sample allocation and the corresponding SD function for natural images to accurately predict the possible compressed sensing performance gains. We further adopt Som and Schniter’s turbo message passing approach to integrate the bandwise sampling with the exploitation of the hidden Markov tree structure of wavelet coefficients. Natural image simulation confirms the theoretical improvements and the effectiveness of bandwise sampling.

Index Terms—Sample distortion function, bandwise sampling, sample allocation, turbo decoding

I. INTRODUCTION

TRADITIONALLY in compressed sensing a lot of work has been done in developing reconstruction algorithms assuming the optimality of the homogeneous random sensing matrix. There has recently been more attention on tailoring the sensing matrix in accordance with the signal of interest. We focus on designing a block diagonal measurement matrix for wavelet representation of natural images which falls under the general scope of bandwise sampling.

Donoho pioneered the use of bandwise sampling for compressed sensing in his original paper [1]. Tsaig further expanded the idea through the concept of two-gender CS, which randomly samples the fine-scale wavelet coefficients while fully samples in the coarse-scale domain [2]. Relatively better reconstruction quality is empirically shown over the homogeneous Gaussian sensing matrix while both of them failed to provide a systematic sample allocation method. Optimizing the bandwise sample allocation of the sensing matrix was originally considered in [3] with the aim of minimizing the reconstruction uncertainty in terms of the entropy of the CS

approximation. However, quantifying the uncertainty is not easy and the authors are obliged to resort to an ad hoc solution.

In fact, the notion of optimized bandwise sampling dates back much further and was instrumental in Kashin’s proof of the optimal rates of approximation (n-widths) for certain classes of smooth function [4], which was a key inspiration for the theory of compressed sensing [1]. Specifically, bandwise sampling forms the basis of Maiorov’s discretization theorem which relates function n-widths to the n-widths of a sequence of finite dimensional ℓ_p balls [5].

In other recent work Krzakala et al. [6] explored a different aspect of selecting a good measurement matrix. As one essential component, the block diagonal spatially-coupled sensing matrix was used to reach the fundamental undersampling limit of compressed sensing with almost perfect reconstruction [6], [7]. However, to achieve the ground-breaking improvement, a first order phase transition must be present. Simply put, the insignificant components of the compressive signal must be extremely small (10^{-6} of the large components in our signal model). We do not observe this level of compressibility in natural images and so this approach is not practical for the compressed sensing of real images.

Main Contributions

In this paper we begin by proposing the sample distortion (SD) function with the aim of assessing the performance of different encoding and decoding methods quantitatively in terms of the expected mean squared error (MSE) distortion. Within the stochastic compressive sensing setting, we employ two compressive statistical models: the generalized Gaussian distribution (GGD) and the two-state Gaussian mixture distribution (GMD). Both of the models have been used for imaging previously e.g. [8], [9], [10], [11]. As a broad definition, the SD function is applicable to any encoder-decoder pair, e.g. the Gaussian homogeneous encoder with the linear ℓ_2 decoder or the ℓ_1 minimum CS decoder. We mainly investigate the SD function for the Bayesian optimal approximate message passing (BAMP) decoder [12], [13]. The AMP algorithm admits a rigorous analysis in the large system limit and naturally provides the theoretical basis for the SD function of CS decoders [14], [15] when used together with the Gaussian random encoder.

In order to understand the SD function better we next derive a simple SD lower bound on the achievable MSE

performance of any linear encoder-CS decoder pair in terms of the differential entropy of the source. A generally tighter model based bound is further derived specifically for both GGD and GMD by leveraging the lower bound for a Gaussian source. Finally we show that the SD function is necessarily convex. This allows us to introduce a hybrid convexified CS encoder-decoder system. Specifically, we show that by randomly throwing away components of the source, a better SD performance can be achieved as the convex combination of the CS decoder and the trivial decoder $\hat{\mathbf{x}} = 0$ in the low sample rate regime.

The second part of the paper makes a contribution to the understanding of optimizing the bandwise sampling in the multi-resolution statistical image model regime following the idea from [3]. Built upon the bandwise independent wavelet model, we are able to define the SD function for each wavelet band, within which the wavelet coefficients are modelled as i.i.d random variables. By virtue of the convexified SD function for Gaussian encoder-CS decoder pair, the optimal sample arrangement is achieved by performing a greedy sample allocation. Simply put, we allocate samples progressively to the wavelet band with the largest distortion reduction, thus defining the SD function for natural images. We then pursue further that direction to incorporate the wavelet dependencies with the bandwise sampling. The wavelet coefficients of natural images are known to have the persistence across scale (PSA) property [16] which can be modelled using the hidden Markov tree (HMT) structure [8]. We leverage Som and Schniter's recently proposed turbo decoding approach to alternate between the CS decoding and the tree structure decoding [17]. Instead of using a uniform distribution of samples across wavelet bands, we choose the optimized block diagonal sensing matrix to sample independently in the CS decoding procedure. We see that together with the exploitation of the wavelet tree structure via the turbo scheme, the accurate message acquired from the coarse scale bands propagates to the fine scale bands and eventually benefit the reconstruction. Theoretically the sample allocation obtained from the bandwise independent wavelet model is suboptimal. However, actual simulation with natural images indicates that it is a reasonable choice since we show that the empirically best sample allocation for the turbo decoding method is not substantially better.

The remainder of the paper is organized as follows. We set up the sample distortion frame work in Section II, where the SD function for two types of compressive distribution is formulated. The convexified CS decoder is introduced based on the convex property of the SD function. In Section III the SD function is expanded to the multi-resolution image model. The sample allocation for bandwise sampling is proposed for both the bandwise independent assumption and the hidden Markov tree structure. Comparison is made between the achievable distortion rates in the statistical CS setting and those known in the deterministic setting for Besov spaces. A turbo decoding approach is employed for the collaboration between bandwise sampling and the exploitation of the bandwise dependencies. Section IV presents the numerical results to compare different encoder-decoder pairs. We finish the paper with the some discussions and conclusion in Section V.

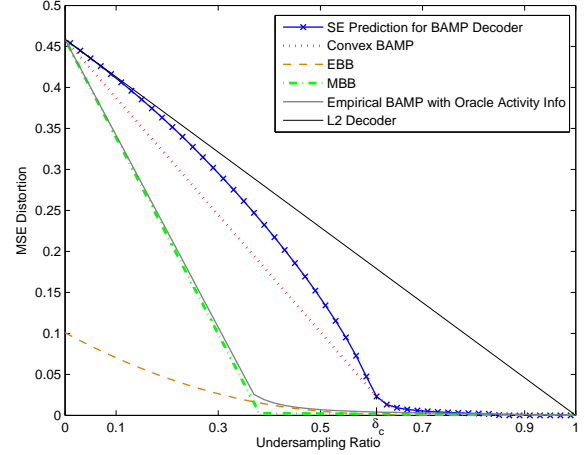


Fig. 1. SD functions for GMD data $p(x) = 0.38 \mathcal{N}(0, 1.198) + 0.62 \mathcal{N}(0, 0.004)$ and lower bounds

II. SAMPLE DISTORTION FRAMEWORK

A. SD function definition

Suppose the signal of interest $\mathbf{x} \in \mathbb{R}^n$ is a random vector (source) with i.i.d components drawn according to the prior distribution $p(x)$. Denote $\Phi \in \mathbb{R}^{m \times n}$, $m < n$ as the measurement matrix or the encoder, and $\mathbf{y} = \Phi \mathbf{x}$ as the underdetermined linear combination of the source. Let $\delta = m/n$ be the undersampling ratio. The goal of statistical compressed sensing is to reconstruct \mathbf{x} using some Lipschitz regular mapping $\Delta : \mathbb{R}^m \rightarrow \mathbb{R}^n$ based on the knowledge of \mathbf{y} , Φ and $p(x)$. In our work, we are interested in the reconstruction quality for certain encoder-decoder pairs (Φ, Δ) at an undersampling ratio δ , which is evaluated by the expected error distortion between the original signal \mathbf{x} and the estimation $\Delta(\Phi \mathbf{x})$:

$$D_{\{\Phi, \Delta\}}(\delta) = \frac{1}{n} \mathbb{E} \|\mathbf{x} - \Delta(\Phi \mathbf{x})\|_2^2 \quad (1)$$

Along the lines of the classical rate-distortion function in the communication field [18], we define a sample distortion function for the compressed sensing setting.

Definition 1: The Sample Distortion (SD) function is defined as the infimum of undersampling ratios for which there is an encoder-decoder pair, (Φ, Δ) , that can achieve an expected distortion D .

$$D(\delta) = \inf_{\Phi, \Delta, n} D_{\{\Phi, \Delta\}}(\delta) \quad (2)$$

Through a slight abuse of terminology, we will also use the term SD function to refer to the minimum distortion level a specific encoder-decoder pair can achieve at a fixed undersampling ratio for a given compressive source. In this paper we will concentrate on the Bayes optimal AMP (BAMP) decoder. We will consider two specific non-Gaussian distributions, the two-state Gaussian Mixture distribution (GMD) and the generalized Gaussian distribution (GGD), to model the compressive random vector.

As the combination of two Gaussian distributions with large and small variance respectively, the GMD model is quite effective at capturing the heavy tailed nature of an approximate sparse signal by adjusting the activity rate λ .

$$\begin{aligned} p_{\text{GMD}}(x) &= p(x, s=1) + p(x, s=0) \\ &= p(s=1)\mathcal{N}(x; 0, \sigma_L^2) \\ &\quad + p(s=0)\mathcal{N}(x; 0, \sigma_S^2) \\ &= \lambda\mathcal{N}(x; 0, \sigma_L^2) + (1-\lambda)\mathcal{N}(x; 0, \sigma_S^2) \end{aligned} \quad (3)$$

A random vector with i.i.d GMD components can be seen as generated from either the small variance Gaussian distribution or from the large one, depending on the hidden states $s = \{0, 1\}$. Since coefficients with small magnitude are expected to dominate the signal domain for compressive signals, it is reasonable to assume $\lambda < 0.5$.

Another popular probabilistic model for compressive data is the generalized Gaussian distribution (GGD). The pdf for the GGD can be written as

$$p_{\text{GGD}}(x) = \frac{\alpha}{2\sqrt{\beta}\sigma\Gamma(\frac{1}{\alpha})} \exp\left(-\left|\frac{x}{\sqrt{\beta}\sigma}\right|^{\alpha}\right) \quad (4)$$

where $\beta = \Gamma(1/\alpha)/\Gamma(3/\alpha)$, σ is the standard deviation and α is the shape parameter. As α goes to zero the distribution has increasingly heavy tails. For images we are typically interested in the GGD with $\alpha \sim [0.3, 1]$ since these distributions provide a good approximation for the distribution of the wavelet coefficients in a given band for natural images.

B. SD function for BAMP

Recent work by Donoho, Maleki and Montannari has shown that the AMP algorithm can achieve the same sparsity undersampling trade-off as the corresponding ℓ_1 convex optimization procedure, but at less computational cost [12]. Furthermore, when the signal prior, $p(x)$, is assumed to be known, the generic AMP algorithm can be tuned optimally by replacing the soft thresholding step with an optimal scalar MMSE estimator [13], [19]. Moreover, the asymptotic MSE behaviour of AMP can be accurately predicted by a state evolution (SE) formalism [15], called the cavity method in the context of statistical physics [7], thus providing a theoretical basis for the SD function for Bayes optimal CS when using a Gaussian encoder. For BAMP decoder, the distortion iteration can be derived from the SE function [19], [7]:

$$D_{k+1} = \mathbb{E}\left\{[F(\tilde{\mathbf{x}} + \sqrt{\frac{D_k}{\delta}}\mathbf{z}; \frac{D_k}{\delta}) - \tilde{\mathbf{x}}]^2\right\} \quad (5)$$

where $\tilde{\mathbf{x}}$ follows the choice of the compressive distribution, $\mathbf{z} \sim \mathcal{N}(0, 1)$ is independent of $\tilde{\mathbf{x}}$, and $D_0 = \mathbb{E}(\tilde{\mathbf{x}}^2)$. The function $F(\cdot)$ is the (non-linear) scalar MMSE optimal estimator for $\tilde{\mathbf{x}}$ given $\tilde{\mathbf{x}} + \mathbf{z}$, which has a close-form expression for GMD [7], [17] and can be solved numerically for GGD. The expectation in (5) is taken with respect to $\tilde{\mathbf{x}}$ and \mathbf{z} and is in general calculated numerically. The SD function for BAMP decoder $D_{\text{BAMP}}(\delta)$ is then given by the fixed point¹ of (5).

¹For the distributions considered in this paper there is only one fixed point, i.e. BAMP exhibits no phase transitions

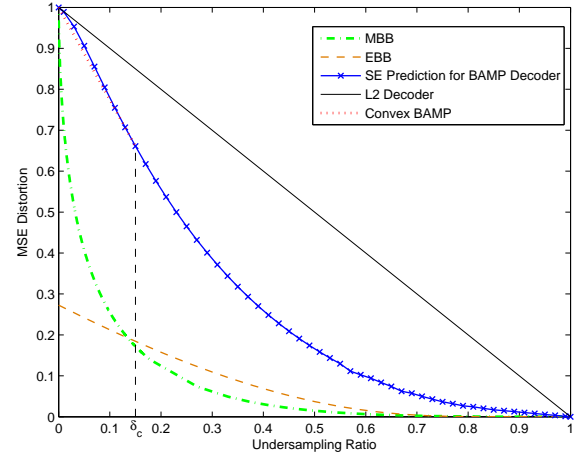


Fig. 2. SD functions for GGD data $\alpha = 0.4$, $\sigma = 1$ and lower bounds

Examples of the theoretical prediction for the SD function of GMD and GGD data using BAMP decoder can be found in Fig. 1 and Fig. 2 respectively.

C. SD Lower bound

To understand the fundamental theoretical limits of CS for compressible distributions, we now derive some bounds for the SD function. We first prove an entropy based bound (EBB) which is a sampling analogy to the classical Shannon Rate Distortion Lower Bound (this result first appeared in the conference paper [20]).

Theorem 1: Let $\mathbf{x} \in \mathbb{R}^n$ be a realization of the random vector $\mathbf{x} = x_1, \dots, x_n$, *i.i.d.* $\sim p(x)$, $\text{Var}(x_i) = 1$ and $h(x_i) < \infty$. Let $\mathbf{y} = \Phi\mathbf{x}$, $\mathbf{y} \in \mathbb{R}^{\delta n}$, $\delta = m/n < 1$. Then for any Lipschitz reconstruction decoder $\Delta : \mathbb{R}^m \rightarrow \mathbb{R}^n$, we have:

$$D_{\Delta}(\delta) \geq (1-\delta)2^{2(h(x)-h_g)/(1-\delta)} \quad (6)$$

where $h_g = \frac{1}{2} \log_2 2\pi e$ is the entropy of a unit variance Gaussian random variable.

The proof is given in appendix A.

The EBB can be easily rescaled to bound the SD performance for distributions with non-unit variance. When the source \mathbf{x} is Gaussian the second term in the lower bound becomes 1. The EBB for a Gaussian distribution reduces to the well known form: $D_{\text{EBB}} = 1-\delta$ which can be shown to be tight. Furthermore when we use the (optimal for Gaussian source) linear estimator, $\hat{\mathbf{x}} = \Phi^\dagger \mathbf{y}$, it is straight forward to show that the SD function, $D_{\ell_2}(\delta)$, has the same form independent of the pdf of the source \mathbf{x} and is achievable with any full rank linear encoder.

While the EBB in Theorem 1 provides a bound on the achievable performance of CS specifically for i.i.d sources, it is not clear how close we can expect to get to it. The EBB for both GMD and GGD data are plotted in Fig. 1 and Fig. 2. We can see that at low undersampling ratios, it is not tight since we expect the SD function, i.e. the MSE, to approach the signal energy as $\delta \rightarrow 0$.

To see this we can define a model based bound (MBB) to compensate for the disadvantage of the EBB. Inspired by the fact that the EBB is tight and achievable for Gaussian source, we resort to the hierarchical Bayesian model to approximate the target compressible distributions. By introducing the variance as a latent variable, the hierarchical representation of a compressible distribution $p(x)$ can be understood as the weighted sum of (possibly infinite) Gaussian distributions.

$$\begin{aligned} p(x) &= \int_0^\infty p(x|\tau)p(\tau) d\tau \\ &= \int_0^\infty \mathcal{N}(x; 0, \tau)p(\tau) d\tau \end{aligned} \quad (7)$$

where $p(\tau)$ is the weight for the Gaussian component $\mathcal{N}(x; 0, \tau)$. The MBB is then derived in the following manner: assume we partition the source \mathbf{x} into different groups according to the variance. For both encoder and decoder, we agree to transmit and reconstruct the source group by group in the descendant order of the variance. For each Gaussian group, its SD performance is tightly bounded by the EBB. Then the lower bound for the whole procedure can be seen as consisting of weighted combination of the EBB of Gaussian components. Thus the MBB has the form:

$$D_{\text{MBB}}(\delta) = \int_0^c \tau p(\tau) d\tau \quad (8)$$

with $\delta = \int_c^\infty p(\tau) d\tau$.

For the GMD model, the MBB is intrinsically a discretized hierarchical Bayesian model with only two Gaussian components. Thus its EBB can be seen as the discretized version of the general form:

$$D_{\text{MBB}}(\delta) = \begin{cases} (1-\lambda)\sigma_S^2 + (\lambda-\delta)\sigma_L^2 & 0 \leq \delta \leq \lambda \\ (1-\delta)\sigma_S^2 & \lambda < \delta \leq 1 \end{cases} \quad (9)$$

For the GGD model, the detailed procedure for inferring its hierarchical Bayesian prior $p(\tau)$ is relegated to appendix B. As we can see in both Fig. 1 and Fig. 2, the MBB is much tighter than the EBB for small undersampling ratios, although neither the MBB nor the EBB dominates for the whole range of the undersampling ratios. The supremum of the two therefore yields a better lower bound for the SD function.

D. Convexity property

In this subsection, we further exploit the similarities with the rate distortion theory to show that the SD function $D(\delta)$ is necessarily convex. We then show a direct application of this to improve the reconstruction quality of the Gaussian encoder-BAMP decoder pair in the low sample-rate regime.

Theorem 2: The SD function $D(\delta)$ is convex.

Proof: Consider two achievable SD points $(\delta_1, D(\delta_1))$ and $(\delta_2, D(\delta_2))$. To prove the SD function is convex, we only need to show the convex combination of the two points is also achievable. Let $\delta_t = t\delta_1 + (1-t)\delta_2$, $0 \leq t \leq 1$. To sample the source $\mathbf{x} \in \mathbb{R}^n$ at the undersampling ratio δ_t , we could split \mathbf{x} into two parts $\mathbf{x} = [\mathbf{x}_1, \mathbf{x}_2]^T$, where $\mathbf{x}_1 \in \mathbb{R}^{tn}$, $\mathbf{x}_2 \in \mathbb{R}^{(1-t)n}$, and apply encoders with undersampling ratio δ_1, δ_2 to $\mathbf{x}_1, \mathbf{x}_2$ respectively. Then the reconstruction of \mathbf{x}_1

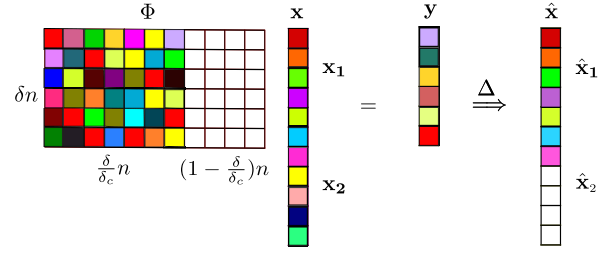


Fig. 3. Hybrid zeroing Gaussian matrix as the convex combination of a trivial decoder $\hat{\mathbf{x}} = 0$ and a BAMP decoder Δ . Elements equal to 0 are represented with white blocks.

and \mathbf{x}_2 has achievable MSE: $tnD(\delta_1)$ and $(1-t)nD(\delta_2)$. So the MSE of the reconstruction of \mathbf{x} is:

$$nD(\delta_t) \leq tnD(\delta_1) + (1-t)nD(\delta_2) \quad (10)$$

Therefore

$$D(t\delta_1 + (1-t)\delta_2) \leq tD(\delta_1) + (1-t)D(\delta_2) \quad (11)$$

The convexity property can be applied to the SD function for any specific encoder-decoder pair. A direct consequence of Theorem 2 is that for a given encoder-decoder pair with a concave SD function between δ_1 and δ_2 ($\delta_1 < \delta_2$), there exists a hybrid system with better SD performance: it can be easily achieved by applying the two encoder-decoders to different portions of the source to get the convex combination of $D(\delta_1)$ and $D(\delta_2)$. A special case is when $\delta_1 = 0$ with the corresponding trivial decoder ($\hat{\mathbf{x}} = 0$) and $\delta_2 = \delta_c$ with δ_c being the crucial undersampling ratio. In this case, instead of sampling the source \mathbf{x} with a full Gaussian matrix, $\Phi \in \mathbb{R}^{n \times n}$, we split \mathbf{x} as before with $\mathbf{x}_1 \in \mathbb{R}^{tn}$ and $\mathbf{x}_2 \in \mathbb{R}^{(1-t)n}$, $t = \delta/\delta_c$. We then sample \mathbf{x}_1 with the Gaussian matrix, $\tilde{\Phi} \in \mathbb{R}^{tn \times tn}$ and reconstruct, while the remaining \mathbf{x}_2 we reconstruct as zero. Since this is equivalent to setting part of the encoder to zero, $\Phi = [\tilde{\Phi}, 0]$, we call this the zeroing procedure, as illustrated in Fig. 3.

Close observation of the SD functions for the Gaussian encoder-BAMP decoder system in Fig. 1 and Fig. 2 reveals that the curves are usually convex for high sampling ratios but concave for low sampling ratios. By applying the hybrid zeroing Gaussian matrix, we achieve a better SD performance for δ below the crucial undersampling ratio δ_c .

The Gaussian sensing matrix has been widely assumed within the CS community to be optimal in terms of CS performance. Indeed this has been proved to be the case for the distributions that exhibit exact sparsity [21]. However, under the assumption that the BAMP achieves the Bayes optimal reconstruction - this would follow, for example, if the replica method could be proved to be rigorous [7] - then the convexified procedure resulting from Theorem 2 indicates this assumption to be false. It also shows that the optimal encoder is related to both the signal property and the corresponding decoding method.

III. SAMPLE DISTORTION FUNCTION FOR STATISTICAL IMAGE MODEL

In this section we leverage the SD functions defined above to study the SD behaviour of the compressive imaging. This enables us to investigate optimal bandwise sampling strategies with a fixed sample budget, in a similar manner to [3], but in terms of the expected distortion of the CS decoder. We begin by introducing the bandwise independent multi-resolution statistical model for natural images.

Natural images are transform compressible: they have more concise representation in the wavelet domain. The wavelet decomposition of an image $f(\mathbf{X})$, $\mathbf{X} \in [0, 1]^2$ has the form [16]:

$$f = \sum_k \mu_{i,k} \phi_{i,k} + \sum_{j \geq i,k} \omega_{j,k} \psi_{j,k} \quad (12)$$

where $\phi_{i,k}$ are the scaling functions, $\psi_{j,k}$ are the prototype bandpass functions such that together they form an orthonormal basis. The variables $\mu_{i,k}$ are in turn the scaling coefficients at scale i and $\omega_{j,k}$ are the wavelet coefficients at scale j . We can group the coefficients into a single vector according to the scale or band $\boldsymbol{\theta} = [\boldsymbol{\mu}_i, \boldsymbol{\omega}_i, \boldsymbol{\omega}_{i+1}, \dots]^T$ and assign each a band index. For simplicity $\boldsymbol{\mu}_i$ is band 0, the coarsest wavelet coefficients group, $\boldsymbol{\omega}_i$, is denoted as band 1, and the rest can be labelled in the same manner. Here we follow [22], [23] and consider a simple statistical model defined directly on the wavelet coefficients. The band 0 is always treated as Gaussian with variance σ_0 , since these coefficients typically exhibit no sparsity. This can be seen as a worse case assumption in terms of its SD function. For the other bands, we model the wavelet coefficients within each band as mutually independent and impose a compressive distribution for each wavelet band. To be specific, $\omega_{j,k}$ at scale j can be modelled as

$$\omega_{j,k} \sim \text{GGD}(0, \sigma_j^2, \alpha_j) \quad (13)$$

or

$$\omega_{j,k} \sim \text{GMD}(\lambda_j, \sigma_{L,j}^2, \sigma_{S,j}^2), \quad (14)$$

where typically for natural images the distributions exhibit a self-similar structure with an exponential decay across scale, i.e. $\sigma_j^2 = 2^{-j\beta} \sigma_0^2$ for the GGD and $\sigma_{a,j}^2 = 2^{-j\beta} \sigma_{a,0}^2$, $a = S, L$ for the two-state GMD for some $\beta > 0$. For the bandwise independent image model, we assume an uniform activity rate λ_j for each wavelet band in spite of the coefficient index. In particular, we define $\lambda_j := \Pr\{s_{j,k} = 1\}$.

A. Bandwise Sampling

To keep things tractable we restrict ourselves to the class of linear encoders, $\mathbf{y} = \Phi \boldsymbol{\theta}$, that are block diagonal and sample the different wavelet bands separately with the following form:

$$\Phi = \begin{pmatrix} \Phi_0 & & & \\ & \Phi_1 & & \\ & & \ddots & \\ & & & \Phi_L \end{pmatrix} \quad (15)$$

where $\Phi_i \in \mathbb{R}^{m_i \times n_i}$, $m_i \leq n_i$ puts m_i measurements to sample the i th band. The equality holds when the i th band

is fully sampled with Φ_i being an identity matrix. Otherwise Φ_i is a possibly zero padded (for convexity) Gaussian random matrix. And $\mathbf{y}_i = \Phi_i \boldsymbol{\omega}_i$ is the CS observation for each block. To derive the SD function for the multi-resolution images, we first consider the L wavelet bands as independent and parallel. The question then is how to allocate a fixed number of samples to the various bands, with the aim of minimizing the total reconstruction distortion. Let us assume for now that m_i, n_i be continuous and $\delta_i = m_i/n_i \in [0, 1]$. The problem is reduced to the following optimization

$$\begin{aligned} \min_{m_i} \quad & \sum_{i=1}^L \sigma_i^2 n_i D_i(m_i/n_i) \\ \text{s.t.} \quad & \sum_{i=1}^L m_i = m \text{ and } 0 \leq m_i \leq n_i, \quad i = 1, \dots, L. \end{aligned} \quad (16)$$

where D_i is the (convex) SD function for band i normalized to have unit variance. Using Lagrange multipliers, we construct the objective function

$$\begin{aligned} L = & - \sum_i \sigma_i^2 n_i D_i(m_i/n_i) \\ & - \lambda \left(\sum_i m_i - m \right) \\ & - \sum_i \mu_i (m_i - n_i) \\ & + \sum_i \nu_i m_i \end{aligned} \quad (17)$$

Differentiating with respect to m_i and setting equal to 0 we have

$$\frac{\partial L}{\partial m_i} = -\sigma_i^2 n_i \frac{\partial D_i}{\partial \delta_i} \cdot \frac{\partial \delta_i}{\partial m_i} - \lambda - \mu_i + \nu_i = 0 \quad (18)$$

or

$$-\sigma_i^2 \frac{\partial D_i}{\partial \delta_i} - \lambda - \mu_i + \nu_i = 0 \quad (19)$$

Define the distortion reduction function as

$$\eta_i(\delta_i) = -\sigma_i^2 \frac{\partial D_i}{\partial \delta_i}, \quad (20)$$

noting that this function is non-increasing in terms of δ_i . Now applying the Kuhn-Tucker (KT) conditions we arrive at:

$$\eta_i(\delta_i) - \lambda - \mu_i + \nu_i = 0, \quad (21)$$

with

$$\mu_i(n_i - m_i) = 0, \quad \mu_i \geq 0, \quad (22)$$

and

$$\nu_i m_i = 0, \quad \nu_i \geq 0. \quad (23)$$

We therefore have three cases for the distortion reduction function. First, if $0 < m_i < n_i$ then $\mu_i = \nu_i = 0$ and the undersampling ratio, δ_i , is set so that $\eta_i(\delta_i) = \lambda$. Next suppose that $m_i = n_i$ so that $\delta_i = 1$. In this case, the KT conditions imply that

$$\eta_i(\delta_i) \geq \lambda, \quad \forall \delta_i \quad (24)$$

In the final case we have $m_i = 0$ and $\delta_i = 0$. Here the KT conditions imply:

$$\eta_i(\delta_i) \leq \lambda, \quad \forall \delta_i \quad (25)$$

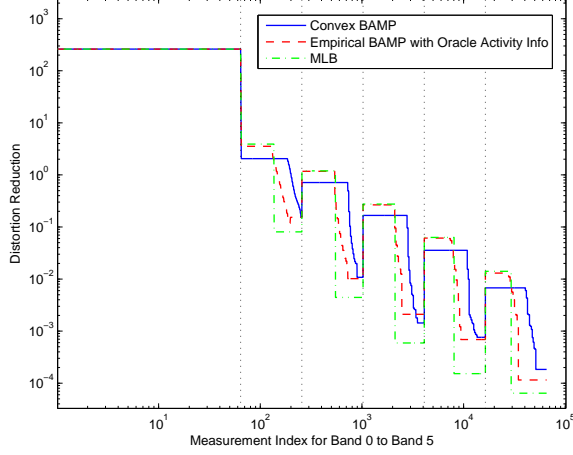


Fig. 4. Distortion reduction function of 6 bands db2 wavelet decomposition of cameraman image using GMD model (including the low-pass band). The statistics is reported in Table I.

This gives us an optimal sample allocation strategy which is similar to the reverse water-filling idea in rate distortion theory [24]. We allocate samples to the band with the greatest distortion reduction value until another band has a greater one or that band has been fully sampled. The procedure is stopped when the total distortion reaches the desired level.

To apply this idea to natural images we need to take account of the fact that m_i , n_i and L are all discrete and finite. Thus we define a discretized distortion reduction (DR) function for each wavelet band.

$$\eta_i(m_i) = \sigma_i^2 [D_i(m_i/n_i) - D_i((m_i + 1)/n_i)] \quad (26)$$

Suppose that m_i samples have been allocated to the i th band. The DR function gives the amount of distortion decreased by adding one more sample to that band. Then the number of samples allocated to the band i is

$$m_i = \begin{cases} 0 & \text{if } \max \eta_i(m_i) < \kappa \\ n_i & \text{if } \min \eta_i(m_i) > \kappa \\ \hat{m}_i \text{ s.t. } \eta_i(\hat{m}_i) = \kappa & \text{otherwise} \end{cases} \quad (27)$$

where κ is chosen so that $\sum_i m_i = m$. With a convex SD function, the optimal allocation is again achieved by performing a greedy sample allocation strategy. The DR function for a six band db2 decomposition based on a multi-resolution two-state GMD fitted to the wavelet coefficients of the cameraman image is illustrated in Fig. 4. One thing worth noting is that neither the convexity property nor the resulting greedy sample allocation method is restricted to the form of the decoder. For example the optimized bandwise sensing matrix can be designed in the same manner for the CS ℓ_1 decoder and the ℓ_2 decoder.

B. Comparison to the Theory of Widths

In [22], parallels are drawn between the statistical wavelet model we have considered here and the family of Besov function spaces. In particular, the authors argue that under

appropriate conditions realizations drawn from the GMD or GGD based wavelet model almost surely lie in an associated Besov space. It is therefore interesting to explore the similarities and differences between the achievable distortion rates derived here and those known in the deterministic setting for Besov spaces.

1) *n-widths of Besov spaces* : Consider the Lipschitz class of r -smooth functions on the interval $[0, 1]$ and the unit ball, B_p^r , defined as:

$$B_p^r := \{f : \|f^{(r)}\|_p \leq 1\} \quad (28)$$

where $f^{(r)}$ denotes the r th derivative of f and the L_p ball acts as the deterministic counterpart to the coefficient prior above.

The ℓ_2 error of the best n -dimensional linear approximation for these spaces is known to scale as $\sim n^{-r+1/p-1/2}$ for $1 \leq p \leq 2$ [25, Chapter 14, Theorem 1.1]. In contrast, the ℓ_2 error for the best CS reconstruction is characterized by the Gelfand width of B_p^r which can be written as:

$$d^n(B_p^r) := \inf_{\Phi} \sup_h \{\|h\|_2, h \in \mathcal{N}(\Phi) \cap B_p^r\}. \quad (29)$$

and measures the uncertainty in B_p^r within the null space of Φ . Here, for $1 \leq p \leq 2$ the best CS approximation error decays at the faster rate of $\sim n^{-r}$, i.e. inversely proportional to the smoothness [25, Chapter 14, Theorem 1.1]. This result was derived in Kashin's seminal paper [4], which is better known in the CS community for accurate bounds for the n -widths of l_p balls in \mathbb{R}^n .

2) *Similarities and differences*: Interestingly Kashin's result relied on a discretization theory of Maiorov [5] that uses a similar bandwise sampling to our own. Specifically Maiorov uses a subband decomposition of spline spaces to bound the n -width of B_p^r in terms of a weighted sum of finite dimensional n -widths for the individual subbands - effectively performing a bandwise sampling. Furthermore in both the deterministic and stochastic settings the allocation scheme is broadly the same: fully sample the first few low resolution subbands; then partially sample a number of intermediate subbands; and finally set coefficients of all the higher resolution subbands to zero. However, in Kashin's theory, the number of partially sampled subbands grows as the distortion decreases and, indeed, it is this that accounts for the different rate of approximation compared with the best linear approximation. In contrast, in the sample allocation framework, the number of partially sampled bands, P , is bounded by the range of the distortion reduction function:

$$P < \beta \log_2(\eta(0)/\eta(1)). \quad (30)$$

For the two-state GMD model this bound is finite since from the MBB we can deduce that:

$$\frac{\eta(0)}{\eta(1)} < \frac{\sigma_{L,0}^2}{\sigma_{S,0}^2} \quad (31)$$

Note the same bound applies to the SD function for the MBB oracle decoder where the bandwise sampling is optimal. Hence, the fact that we do not get a growing number of partially sampled subbands implies that in the large system limit the CS approximation error will decay at the same

rate as for the best linear approximation. We can therefore conclude that the gains in CS solutions over optimal linear approximation for such a model are fundamentally limited. We can see this, for example, in Fig. 4 where we would only ever partially sample at most 3 subbands for the convexified BAMP decoder.

C. Incorporating Tree Structure

Until now we have developed a tractable sample allocation method for a multi-resolution image model by assuming the independence of the wavelet band. In this subsection we look beyond basic sparsity and incorporate the wavelet dependencies. We model the wavelet coefficients with the GMD and impose the hidden Markov tree (HMT) structure to the hidden states as in [8]. To be specific, with the hidden states at the coarsest scale (band 1) being the "root", we connect each wavelet hidden state to the four "child" wavelet states below it to form the image quadtree (see Fig. 5). The PSA property states that the coefficient is more likely to be small if its parent is small; similarly, it is likely to be large if its parent is large [16]. In this case, the activity rate $\lambda_{j,k}$ for $\omega_{j,k}$ depends on the activity rate of its parent on scale $j-1$, λ_{j-1,p_k} , and the transition probabilities across scales.

$$\begin{aligned} \lambda_{j,k} = & p(s_j = 1 | s_{j-1} = 1) \lambda_{j-1,p_k} \\ & + p(s_j = 1 | s_{j-1} = 0) (1 - \lambda_{j-1,p_k}) \end{aligned} \quad (32)$$

By incorporating the HMT decoding, we can provide a better estimation of $\lambda_{j,k}$ for each wavelet coefficient instead of using an identical λ_j over the coefficient index k , thus improving the reconstruction quality.

We first review the core principles of Som and Schniter's TurboAMP decoding method [17]. Let $\omega = [\omega_1, \omega_2, \dots, \omega_L]^T$ denote the collection of the wavelet coefficients of different bands and $\mathbf{s} = [\mathbf{s}_1, \mathbf{s}_2, \dots, \mathbf{s}_L]^T$ the corresponding hidden states vector. Assume $\mathbf{y} = [\mathbf{y}_1, \mathbf{y}_2, \dots, \mathbf{y}_L]^T$ is the CS observation vector using the block diagonal sensing matrix. In the Bayesian compressed sensing setting, the reconstruction of ω from \mathbf{y} is interpreted as approximating the posterior mean of the density $p(\omega | \mathbf{y})$:

$$\begin{aligned} p(\omega | \mathbf{y}) &= \sum_{\mathbf{s}} \prod_{j=0}^L p(\omega_j | \mathbf{y}_j, \mathbf{s}) p(\mathbf{s}) \\ &= \sum_{j=0}^L \frac{1}{z_j} \sum_{\mathbf{s}} p(\mathbf{s}) \prod_{k=1}^{n_j} p(\omega_{j,k} | s_{j,k}) \prod_{t=1}^{m_j} p(y_{j,t} | \omega_j) \end{aligned} \quad (33)$$

where z_j ensures the normalization $\int p(\omega_j | \mathbf{y}_j) = 1$. The factor graph plotted in Fig. 5 visualizes this global function [26], [27]. Exact computation of $p(\omega | \mathbf{y})$ is NP hard due to the dense and loopy structure of the factor graph. Instead we split the factor graph along the dashed line into two subgraphs as in [17] and calculate the marginal posterior $p(\omega_{j,k} | \mathbf{y}_j)$. The essence of turbo decoding is to exchange the local belief of the hidden states $s_{j,k}$ between AMP decoding and HMT decoding alternately, by treating the "extrinsic" information

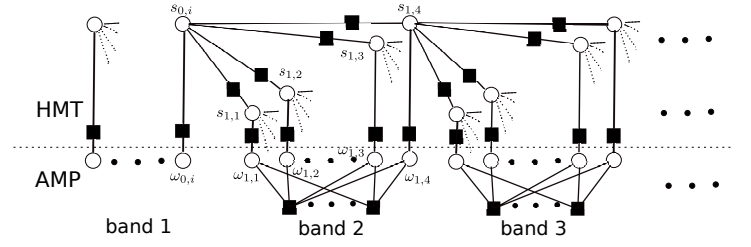


Fig. 5. Factor graph for bandwise sampling with HMT decoding. The upper graph illustrates a quadtree structure of the wavelet hidden states. The lower graph is the bandwise independent random mixing.

on $s_{j,k}$ from one decoding procedure as prior for the other decoding procedure. Here, unlike [17], the AMP decoder is bandwise independent due to the block diagonal form of Φ . The interaction across different wavelet bands only comes from the HMT decoding. For a fully sampled wavelet band (e.g. band 1), the extrinsic information $\hat{\lambda}_{j,k}$ passing from the BAMP decoding to the HMT decoding as the prior can be obtained as [17]:

$$\begin{aligned} \hat{\lambda}_{j,k} &= \frac{p(\omega_{j,k} | s_{j,k} = 1)}{p(\omega_{j,k} | s_{j,k} = 1) + p(\omega_{j,k} | s_{j,k} = 0)} \\ &= \frac{\mathcal{N}(\omega_{j,k}; 0, \sigma_{j,L}^2)}{\mathcal{N}(\omega_{j,k}; 0, \sigma_{j,L}^2) + \mathcal{N}(\omega_{j,k}; 0, \sigma_{j,S}^2)} \end{aligned} \quad (34)$$

We denote $\hat{\lambda}_{j,k}$ as the oracle activity rate for $\omega_{j,k}$. The accurate information of the activity rate of the parent hidden states can then propagate through the HMT decoding, improve the estimation of the activity rate of their children states (the partially sampled bands, e.g. band 2, band 3) and benefit the final reconstruction.

It is obvious that the SD function for the bandwise independent image model is not appropriate for the turbo decoding scenario since it does not take the HMT decoding into consideration. To see the impact of HMT decoding, we plotted an empirical SD curve for BAMP decoder with the oracle extrinsic information of the hidden states in Fig. 1. The empirical curve is generated from the Monte Carlo simulations with synthetic GMD data. To be specific, we use the $\hat{\lambda}_{j,k}$ in (34) instead of λ_j for the scalar MMSE estimator of each synthetic GMD component. Fig. 1 demonstrates that providing the BAMP decoder with extra hidden states information dramatically improves the reconstruction quality with the SD function lying very close to the lower bound. On the same principle, we could establish the DR function with the oracle activity information for the multi-resolution image model, as shown in Fig. 4, and the corresponding SD function. To clarify the terminology, we denote the sample allocation for bandwise independent wavelet model as SA and the one based on the HMT model as HSA. We should note here that neither SA nor HSA is optimal for turbo decoding. The problem with SA is that it tends to undersample the fine scale bands since they contain less energy than the coarse bands when treated independently. While HSA is served as the benchmark by assuming we have the oracle hidden state information for each wavelet coefficient. The optimal sample allocation for turbo decoding should combine the merits of both SA and HSA.

IV. NATURAL IMAGE EXAMPLE

The last section illustrates that the multi-resolution SD function for natural images can accurately predict the reconstruction distortion with the proposed bandwise sample allocation scheme. It also demonstrates the effectiveness of the sample allocation in terms of improving the image reconstruction quality, in spite of the choice of decoder. All simulations are performed on the 256×256 grayscale "cameraman" image as an example. We consider the haar wavelet and db2 wavelet decomposition of "cameraman" to model the image statistics. Similar results are found in a wide range of other images.

A. set up

We begin by estimating the parameters for both GGD and GMD to set up the multi-resolution statistical model. Table I shows the GGD and GMD parameter estimation for the 6 bands db2 wavelet coefficients of cameraman using moment matching [23] and EM algorithm [28] respectively.

subband		b_0	b_1	b_2	b_3	b_4	b_5
GGD	α	2	0.7	0.4	0.3	0.3	0.4
	σ^2	261.4383	2.0822	0.4559	0.0902	0.0167	0.0033
	λ	1	0.4155	0.5309	0.4842	0.3664	0.2792
GMD	σ^2	261.4383	4.4215	0.8542	0.1856	0.0453	0.0115
	σ_L^2		0.3331	0.0038	0.0004	0.0002	0.0001
	σ_S^2						

TABLE I
STATISTICS FOR DB2 WAVELET COEFFICIENTS OF CAMERAMAN

As previously stated, the scaling coefficients are modelled as Gaussian with the shape parameter being 2 for the GGD and the activity rate for hidden states being 1 for the GMD. Variances for the wavelet bands exhibit an exponential energy decay for both distribution models. Given the parameter estimation, we are able to generate the image SD function and the subsequent bandwise sample allocation using the aforementioned method.

The performance of the proposed bandwise sampling matrix is compared with the homogeneous Gaussian sensing matrix and the two-gender sensing matrix. The former uniformly distributes samples across all bands while the latter fully samples the scaling band and uniformly allocates the remaining samples to all the wavelet coefficient bands. To show the sample allocation method is not restricted to the form of the decoders, we consider three reconstruction options: the linear ℓ_2 decoder, the CS ℓ_1 decoder, and the BAMP decoder. The SPGL1 toolbox² is used to implement the ℓ_1 decoder. Its SD function can also be derived using the SE formalism [15]. Both the ℓ_2 and the ℓ_1 decoder are considered for the GGD and the GMD model. Since there is no close form MMSE estimator for the GGD data, the BAMP decoder is only applied to the GMD model. The detailed algorithm can be found in [17], [7].

Within the GMD regime, we further leverage the quadtree structure of the hidden states through the turbo scheme. Three different sample allocations are examined when incorporating with the HMT decoding: SA, HSA, and the empirically optimized sample allocation, or ESA. The ESA is obtained by

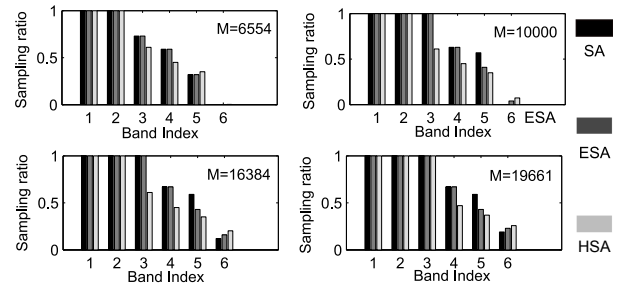


Fig. 6. Sample allocation per band for db2 wavelet with the GMD model. SA: sample allocation based on the bandwise independent model. HSA: sample allocation with the oracle activity information. ESA: empirically achieved best sample allocation for turbo decoding.

manually moving a minimum of 100 samples from other bands to the finest wavelet band based on the SA to balance to total distortion. For the turbo decoding, the extrinsic information $\hat{\lambda}_{j,k}$ defined in (34) is assigned as the activity prior for the HMT structure when band j is fully sampled. An identical activity prior λ_j as reported in Table I is used for partially sampled bands. Other hyperparameters to initialize the HMT decoding are set in accordance with the recommendation in [17]. For various choices of sample allocations, we ran 20 turbo iterations, within which 50 BAMP iterations are performed.

For quantitative comparison, the signal to distortion ratio (SDR) is used for both theoretical performance prediction and the experiments with the image. We examined cameraman at 4 different undersampling ratios : 10%,15,26%,25% and 30% associated with $m = 6554, 10000, 16384, 19661$ noiseless measurements. The sample allocation for six bands db2 wavelet decomposition of cameraman with the GMD model is reported in Fig. 6. We see that the scaling band and the coarse wavelet band always have the priority over the fine wavelet bands in terms of allocating samples. The same sampling pattern is also observed for the haar wavelet decomposition. And the ESA is the balance between SA and HSA, as expected.

B. results comparison

The reconstruction performance comparison among different choice of encoder-decoder pairs is twofold. First, the wavelet bands are assumed as mutually independent. We model the db2 wavelet coefficients of the cameraman image with both GGD and GMD model. The SDR results for different decoders with and without sample allocation are shown in Fig. 7 and Fig. 8 for the GGD and the GMD respectively. The theoretical distortion prediction and lower bound are plotted as lines. And the actual distortion obtained with the cameraman image are represented as dots. From the figures, we observed that the SD functions predict the expected distortion quite accurately for all three choices of the decoder with the corresponding optimized sample allocation. The advantage over the homogeneous matrix and the two-gender matrix can be easily seen: there is roughly 4db SDR gain over Uniform+L1 and 2 Gender+L1 at 10% and 15% Nyquist rate and 2db gain when $\delta = 25\%, 30\%$ for both

²<http://www.cs.ubc.ca/labs/scl/spgl1/index.html>

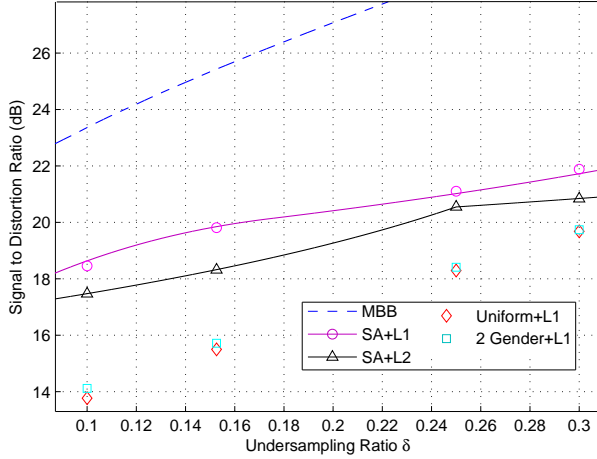


Fig. 7. SDR comparison of different encoder-decoder pairs for cameraman db2 wavelet with bandwise independent GDD model

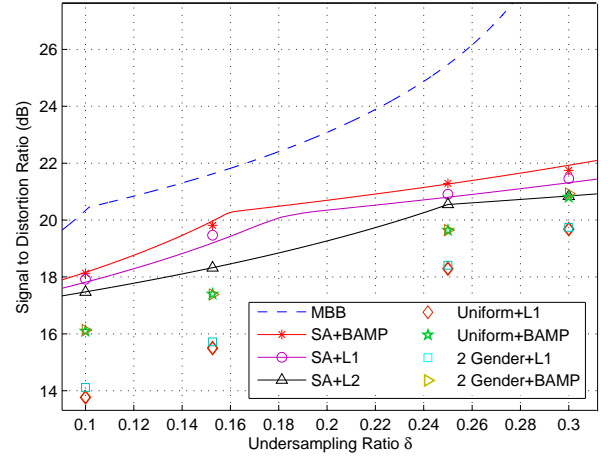


Fig. 8. SDR comparison of different encoder-decoder pairs for cameraman db2 wavelet with bandwise independent GMD model

statistical models. For GMD with the BAMP decoder, there is an average of 2db gain over the unstructured sensing matrix for the GMD model. The ℓ_1 decoder always performs better than the ℓ_2 decoder. And the BAMP decoder is the best among the three. The reason is that the ℓ_1 decoder makes use of the sparsity property. And the BAMP decoder is provided with the signal statistical information. Similar results are also observed for the haar wavelet decomposition.

Secondly, the HMT structure of the wavelet bands are taken into consideration. The comparison for different sample allocation proposals are made within the turbo decoding regime. We use the GMD model and the BAMP decoder for both haar wavelet and db2 wavelet coefficients. It is the joint use of optimized bandwise sampling and the turbo approach that delivers by far the best SDR performance, as evident in Fig. 9 and Fig. 10. Again, sample allocation shows its importances when there is a tight budget of samples: even without the turbo decoding procedure, SA+BAMP is 2db better at $\delta = 0.1$ and 1db better at $\delta = 0.15$ than Uniform+TurboAMP. We observed that the ESA is only slightly better than the independent model based sample allocation. It means that we should guarantee the coarse-scale bands are fully samples when we are short of samples since their energy dominates the whole image. Even when we have the luxury of manipulating samples, the benefit from HMT decoding is limited because of the energy boundary of the fine-scale bands.

The 256×256 cameraman image along with the reconstructed images by different encoder-decoder pairs are visualized in Fig. 11 at the undersampling ratio $\delta = 15\%$. It further confirms the improvement achieved by implementing the bandwise sampling strategy while the gain of adding the HMT ingredient is not visibly substantial.

V. CONCLUSION

The main contributions of this paper are the set-up of the sample distortion framework for statistical compressed sensing, the investigation of its property and its extension

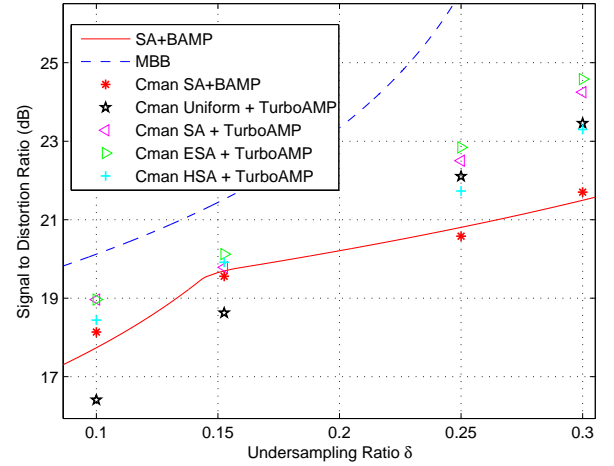


Fig. 9. SDR comparison of different sample allocation with turbo decoding for cameraman haar wavelet coefficients with GMD model.

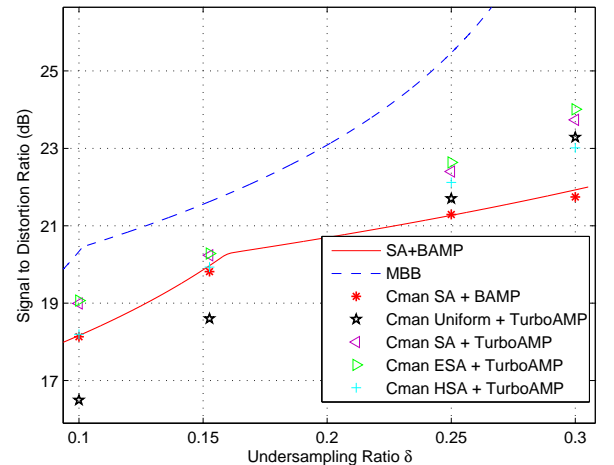


Fig. 10. SDR comparison of different sample allocation with turbo decoding for cameraman db2 wavelet coefficients with GMD model.

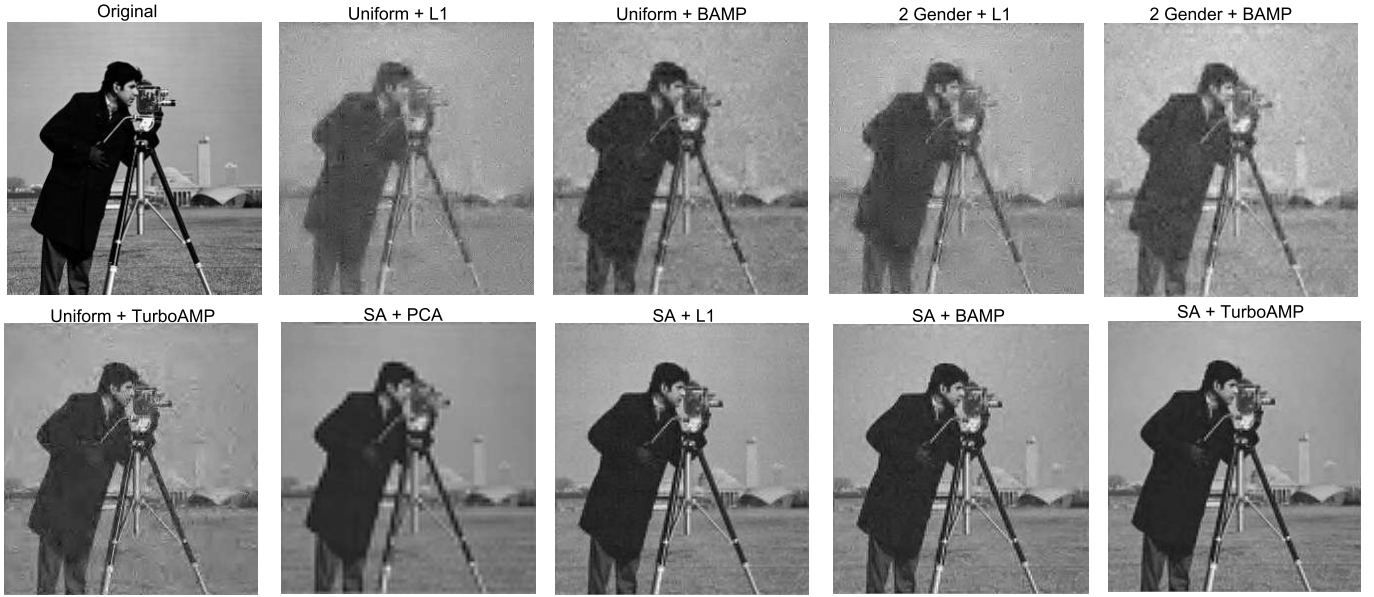


Fig. 11. Reconstruction using 10000 (15%) samples of the 256×256 cameraman image with different encoder-decoder pairs. The GMD is used to model the db2 wavelet coefficients statistics.

extension to multi-resolution statistical image models. We have derived a tractable sample allocation method for minimizing the reconstruction distortion and shown that it provides an accurate prediction of the achievable SD performance for natural images. Finally, inspired by the turbo decoding approach of Som and Schinter, we have explored the use of tree structured sparsity within the optimized bandwise sampling framework. Various encoder-decoder combination examined with the cameraman image illustrates the merit of bandwise sampling, especially in the regime of very low undersampling ratios. Future work will explore the possibility of adaptive sample allocation to get closer to the SD lower bound.

APPENDIX A PROOF OF THEOREM 1

Without loss of generality we will assume that Φ is an orthogonal projection operator and we denote by Φ^\perp the orthogonal projection onto the null space of Φ . We can then split the signal \mathbf{x} into its observed and unobserved components: $\mathbf{y} = \Phi\mathbf{x}$ and $\mathbf{z} = \Phi^\perp\mathbf{x}$. Since we directly observe \mathbf{y} we need only consider the component of the decoder that estimates \mathbf{z} , $\Delta^{(z)} : \mathbb{R}^m \rightarrow \mathbb{R}^{n-m}$. We can then estimate \mathbf{x} as:

$$\hat{\mathbf{x}} = \Delta(\mathbf{y}) = \Phi^T \mathbf{y} + [\Phi^\perp]^T \Delta^{(z)}(\mathbf{y}) \quad (35)$$

We can further write the squared error distortion in terms of $\Delta^{(z)}(\mathbf{y})$ as

$$D = \frac{1}{n} \int p(\mathbf{y}) \int p(\mathbf{z}|\mathbf{y}) \|\mathbf{z} - \Delta^{(z)}(\mathbf{y})\|_2^2 d\mathbf{z} d\mathbf{y} \quad (36)$$

Now consider the following decomposition of the differen-

tial entropy $h(\mathbf{x})$ of the vector \mathbf{x} :

$$\begin{aligned} h(\mathbf{x}) &= h(\mathbf{y}) + h(\mathbf{z}|\mathbf{y}) \\ &= h(\mathbf{y}) + h(\mathbf{z} - \Delta^{(z)}(\mathbf{y})|\mathbf{y}) \\ &\leq h(\mathbf{y}) + h(\mathbf{z} - \Delta^{(z)}(\mathbf{y})) \\ &\leq \frac{m}{2} \log_2 2\pi e + \frac{n-m}{2} \log_2 2\pi e n D / (n-m) \end{aligned} \quad (37)$$

where we have used the following observations

- (line 2) The decoder is a deterministic function of \mathbf{y} and therefore the differential entropy of $h(\mathbf{z} - \Delta^{(z)}(\mathbf{y})|\mathbf{y}) = h(\mathbf{z}|\mathbf{y})$.
- (line 3) The conditional entropy is bounded by the marginal entropy: $h(\mathbf{x}|\mathbf{y}) \leq h(\mathbf{x})$.
- (line 4) The entropy of a random variable with a fixed covariance is bounded by the entropy of a Gaussian with the same covariance. Similarly the entropy of a random vector $\mathbf{v} \in \mathbb{R}^{n-m}$ under the constraint that $\mathbb{E}\{\mathbf{v}^T \mathbf{v}\} = nD$ is bounded by the entropy of a Gaussian random vector with covariance $\frac{nD}{(n-m)I}$.

The principle here is that the optimal projection should maximize the entropy of the observed component $h(\mathbf{y})$ while the decoder, $\Delta(\mathbf{y})$, should minimize the distortion possible. This is similar to the concept of information sensing proposed in [3].

Substituting $\delta = m/n$ into (37) gives:

$$h(x) \leq \frac{1-\delta}{2} \log_2 2\pi e \frac{D}{1-\delta} + \frac{1}{2} \log_2 2\pi e \quad (38)$$

where we have used the i.i.d assumption to write $h(\mathbf{x}) = nh(x)$. This can then be rearranged to give the EBB.

APPENDIX B

DERIVATION OF THE HIERARCHICAL BAYESIAN MODEL FOR THE GGD

Here, we derive the hierarchical Bayesian model to describe the GGD, which is then used to bound the MSE performance described in the main text in Sec. II-C. We introduce two latent variables c_1 and c_2 to simplify the expression of GGD:

$$c_1 = \frac{\alpha}{2\sqrt{\beta}\sigma\Gamma(\frac{1}{\alpha})} \quad c_2 = (\sqrt{\beta}\sigma)^\alpha \quad (39)$$

Then the pdf of GGD can be written as

$$p_{\text{GGD}}(x) = c_1 \exp\left(-\frac{|x|^\alpha}{c_2}\right) \quad (40)$$

Let $p(x|\tau) = \mathcal{N}(x; 0, \tau)$. To establish the hierarchical model, we need to find the prior $p(\tau)$ which satisfies:

$$\int_0^\infty \mathcal{N}(x; 0, \tau) p(\tau) d\tau = c_1 \exp\left(-\frac{|x|^\alpha}{c_2}\right) \quad (41)$$

Using the substitution $g(\tau) = \frac{1}{\sqrt{2\pi\tau}} p(\tau)$, $m = \frac{x^2}{2}$ and $t = \frac{\sqrt{2}^\alpha}{c_2}$, the question becomes solving $g(\tau)$ subject to

$$\int_0^\infty \exp\left(-\frac{m}{\tau}\right) g(\tau) d\tau = c_1 \exp(-tm^{\frac{\alpha}{2}}) \quad (42)$$

let $z = \frac{1}{\tau}$ and $G(z) = g(\tau)|_{\tau=\frac{1}{z}}$, we further transform the problem to find $G(z)$ subject to

$$\int_0^\infty \exp(-zm) \frac{G(z)}{z^2} dz = c_1 \exp(-tm^{\frac{\alpha}{2}}) \quad (43)$$

Applying the integral formula [29]: if $\int_0^\infty e^{-zt} y(t) dt = f(z)$, then $y(t) = \mathcal{L}^{-1}(f(z))$, we obtain

$$\frac{G(z)}{z^2} = c_1 \mathcal{L}^{-1} \exp\left(-\frac{x^\alpha}{c_2}\right) \quad (44)$$

where $\mathcal{L}^{-1}(\cdot)$ is the inverse Laplace transform. The inversion of Laplace transform in (44) can be solved numerically [30]. From here we obtain the MBB for the GGD data in Fig. 2.

REFERENCES

- [1] D. Donoho, "Compressed sensing," *IEEE Trans. on Information Theory*, vol. 52, pp. 1289–1306, 2006.
- [2] Y. Tsaig, "Sparse solution of underdetermined linear systems: algorithms and applications," Ph.D. dissertation, Stanford University, 2007.
- [3] H. S. Chang, Y. Weiss, and W. Freeman, "Informative sensing of natural images," in *Image Processing (ICIP), 2009 16th IEEE International Conference on*, nov. 2009, pp. 3025–3028.
- [4] B. S. Kashin, "Diameters of some finite-dimensional sets and classes of smooth functions," *Math. USSR Izvestiya*, vol. 11, pp. 317–333, 1977.
- [5] M. Maiorov, "Discretization of the diameter problem," *Uspekhi Mat. Nauk*, vol. 30, pp. 179–180, 1975.
- [6] F. Krzakala, M. Mézard, F. Sausset, Y. Sun, and F. Zdeborová, "Statistical physics-based reconstruction in compressed sensing," arXiv:1109.4424, 2011.
- [7] F. Krzakala, M. Mézard, F. Sausset, and Y. Sun, "Probabilistic reconstruction in compressed sensing: Algorithms, phase diagrams, and threshold achieving matrices," arXiv:1206.3953v1 [cond-mat.statmech], 2012.
- [8] M. Crouse, R. Nowak, and R. Baraniuk, "Wavelet-based statistical signal processing using hidden markov models," *Signal Processing, IEEE Transactions on*, vol. 46, no. 4, pp. 886–902, apr 1998.
- [9] M. Duarte, M. Wakin, and R. Baraniuk, "Wavelet-domain compressive signal reconstruction using a hidden markov tree model," pp. 5137–5140, 31 2008–april 4 2008.
- [10] P. Moulin and J. Liu, "Analysis of multiresolution image denoising schemes using generalized gaussian and complexity priors," *Information Theory, IEEE Transactions on*, vol. 45, no. 3, pp. 909–919, apr 1999.
- [11] C. Bouman and K. Sauer, "A generalized gaussian image model for edge-preserving map estimation," *Image Processing, IEEE Transactions on*, vol. 2, no. 3, pp. 296–310, jul 1993.
- [12] D. Donoho, A. Maleki, and A. Montanari, "Message passing algorithms for compressed sensing," arXiv:0907.3574, 2009.
- [13] A. Donoho, D. and Maleki and A. Montanari, "Message passing algorithms for compressed sensing: I. motivation and construction," in *Information Theory Workshop (ITW), 2010 IEEE*, Jan., pp. 1–5.
- [14] M. Bayati and A. Montanari, "The lasso risk for gaussian matrices," *Information Theory, IEEE Transactions on*, vol. 58, no. 4, pp. 1997–2017, april 2012.
- [15] —, "The dynamics of message passing on dense graphs with applications to compressed sensing," *Information Theory, IEEE Transactions on*, vol. 57, no. 2, pp. 764–785, Feb.
- [16] S. Mallat, *A Wavelet Tour of Signal Processing*. San Diego, CA: Academic Press, 1999.
- [17] S. Som and P. Schniter, "Compressive imaging using approximate message passing and a markov-tree prior," *Signal Processing, IEEE Transactions on*, vol. 60, pp. 3439–3448, 2012.
- [18] C. Shannon and W. Weaver, *The mathematical theory of communication*. University of Illinois Press, 1949.
- [19] D. Donoho, A. Maleki, and A. Montanari, "How to design message passing algorithms for compressed sensing," Available: <http://www.ece.rice.edu/mam15/bpist.pdf>, 2011.
- [20] M. Davies and C. Guo, "Sample-distortion functions for compressed sensing," in *Communication, Control, and Computing (Allerton), 2011 49th Annual Allerton Conference on*, sept. 2011, pp. 902–908.
- [21] Y. Wu and S. Verdú, "Optimal phase transitions in compressed sensing," *IEEE Transactions on Information Theory*, vol. 58, no. 10, pp. 6241–6263, 2012.
- [22] H. Choi and R. Baraniuk, "Wavelet statistical models and besov spaces," in *Proc. SPIE*, vol. 3813, 1999, p. 489.
- [23] S. Mallat, "A theory for multiresolution signal decomposition: the wavelet representation," *IEEE Trans. Pattern Anal. Machine Interll.*, vol. 11, pp. 674–693, 1989.
- [24] T. M. Cover and J. A. Thomas, *Elements of Information Theory*, 2nd ed. Wiley-Interscience, July 2006.
- [25] G. G. Lorentz, M. v. Golitschek, and Y. Makovoz, *Constructive approximation : advanced problems*, ser. Grundlehren der mathematischen Wissenschaften. Berlin, New York: Springer, 1996. [Online]. Available: <http://opac.inria.fr/record=b1091520>
- [26] A. Montanari. (2011) Graphical models concepts in compressed sensing. [Online]. Available: [Available:arXiv:1011.4328v3\[cs.IT\]](http://arxiv.org/abs/1011.4328v3).
- [27] F. Kschischang, B. Frey, and H.-A. Loeliger, "Factor graphs and the sum-product algorithm," *Information Theory, IEEE Transactions on*, vol. 47, no. 2, pp. 498–519, feb 2001.
- [28] A. P. Dempster, N. Larid, and D. Rubin, "Maximum likelihood from incomplete data via the em algorithm," *Journal of the royal statistical society. Series B*, vol. 39, pp. 1–38, 1977.
- [29] A. Polyanin and A. V. Manzhirov, *Handbook of integral equations*, 2nd ed. Chapman and Hall/CRC Press, 2008.
- [30] J. Valsa and L. Brancik, "Approximate formulae for numerical inversion of laplace transforms," *Int. Journal for Numerical Modelling: Electronic Networks, Devices and Fields*, vol. 11, pp. 153–166, June 1998.